

# Theory of low-energy electron diffraction for detailed structural determination of nanomaterials: Finite-size and disordered structures

G. M. Gavaza,<sup>1</sup> Z. X. Yu,<sup>1,2</sup> L. Tsang,<sup>3</sup> C. H. Chan,<sup>4</sup> S. Y. Tong,<sup>1</sup> and M. A. Van Hove<sup>1</sup>

<sup>1</sup>*Department of Physics and Materials Science, City University of Hong Kong, Hong Kong*

<sup>2</sup>*Department of Physics, Zhongshan University, Guangzhou 510275, China*

<sup>3</sup>*Department of Electrical Engineering, University of Washington, Seattle, Washington 98195-2350, USA*

<sup>4</sup>*Department of Electronic Engineering, City University of Hong Kong, Hong Kong*

(Received 26 February 2007; published 5 June 2007)

We describe how a recent efficient theory of low-energy electron diffraction (LEED) enables the determination of finite-size and disordered nanostructures. Our cluster approach, called NANOLEED, speeds up the computation to scale as  $n \log n$ , rather than the usual  $n^3$  or  $n^2$ , with  $n$  the number of atoms, for example, thereby making nanostructures accessible. To illustrate this method's capability to determine nanoscale structure, we apply it to calculate LEED intensities for Si nanowires of various lengths and thicknesses as well as for various deviations of these nanowires from the ideal Si bulk structure.

DOI: [10.1103/PhysRevB.75.235403](https://doi.org/10.1103/PhysRevB.75.235403)

PACS number(s): 61.46.-w, 61.14.Dc, 61.14.Hg, 61.48.+c

## I. INTRODUCTION

In two recent papers<sup>1,2</sup> we introduced a method to calculate intensities of low-energy electron diffraction (LEED), called NANOLEED, with an efficiency that allows the structural determination of complex structures such as those of nanomaterials. The capability of the method was exhibited by its application to ordered layers of  $C_{60}$  molecules and carbon nanotubes adsorbed on a Cu(111) surface, as detailed in Ref. 2.

Many nanostructures are not ordered, i.e., not periodic, and we therefore also need to demonstrate the possibility of using LEED in the case of finite-size and disordered nanostructures. To that end, we choose here to formulate the method in a slightly more general fashion and to apply it to silicon nanowires (SiNWs). No LEED measurements are available as yet for SiNWs, or any other individual nanostructures, so this paper will focus on showing the sensitivity of LEED intensities to relevant structural aspects of SiNWs, as a model for nanostructures in general. We will explore various sizes and structural changes of SiNWs, including hydrogen termination of silicon dangling bonds and several nonperiodic distortions. This choice was motivated, in particular, by studies performed with scanning tunneling microscopy (STM) on SiNWs that exhibit a range of sizes, and which are believed to be hydrogen terminated.<sup>3,4</sup> This type of nanowire can be experimentally grown<sup>3</sup> on a highly oriented pyrolytic graphite (HOPG) substrate, and total energy calculations have shown<sup>5</sup> that the stable cross section of a H-terminated SiNW is likely rectangular. Guided by experiment, in particular, STM images,<sup>3</sup> we select a SiNW with a  $[1, 1, -2]$  direction of growth: STM shows its (111) facet exposed, and thus its side facets would have  $\{1-10\}$  orientation. We will assume unreconstructed Si facets, as is observed experimentally due to the H saturation: clearly, "NANOLEED" could be used very well to study details of such facet reconstruction. In this application, we ignore the supporting substrate (HOPG), but it could be included if desired.

Before applying the theory of LEED to nanostructures, we need to ask what will be the nature of the LEED pattern

for isolated nanoparticles and nanowires, from which intensities for analysis should be measured. This will be discussed in Sec. II. One way to focus a LEED experiment on a single nanoscale structure is to use a convergent incident beam.<sup>6</sup> But it is also possible to use conventional collimated beams in the case of ordered overlayers of nanostructures deposited on periodic substrates. Therefore, we will develop in Sec. III a more general formulation of LEED theory that includes both the extremes of convergent beams and traditional collimated beams. Section IV will apply our NANOLEED theory to the case of a variety of silicon nanowires. Conclusions will be listed in Sec. V.

## II. NANOLEED PATTERN

The analysis of LEED intensities has so far focused on surfaces of bulk crystals: these are periodic in two dimensions,<sup>7,8</sup> and sometimes include disordered layers on such periodic substrates.<sup>9</sup>

In the two-dimensional (2D) periodic case, the angular distribution of the diffracted electrons produces a simple and familiar LEED pattern: for an ideal collimated incident beam, it consists of a set of sharp beams that represent the reciprocal lattice of the two-dimensional periodic surface lattice (this ignores inelastic effects such as electron-phonon scattering that produce diffuse intensities near the sharp beams). The beam intensities provide the experimental data to which an unknown surface structure is fitted by theoretical simulation.

With a disordered overlayer, as with defective surfaces, the LEED pattern becomes diffuse, with intensity distributed everywhere between the sharp beams of the periodic part of the structure. For simple cases like lattice-gas disorder (an example is the situation where all adsorbates sit in the same positions relative to the substrate lattice), the diffuse intensities can also be analyzed in terms of local structure of the disordered part of the surface.<sup>9</sup>

The aforementioned patterns also result from ordered or disordered arrays of nanostructures, for example, when these are deposited as an overlayer on a crystalline substrate. We

described such a case recently, namely, an overlayer of  $C_{60}$  buckyballs on Cu(111) ordered in a  $(4 \times 4)$  superlattice.<sup>1,2</sup>

If we wish to study individual nanostructures or nanoscale areas of a surface, one option is to produce a convergent electron beam that exposes only the structure of interest, as proposed earlier under the name convergent-beam LEED.<sup>6</sup> It may be possible to focus a beam down to the nanoscale.<sup>6</sup> Another experimental method to expose a small surface area uses a nearby STM tip to create a narrow beam of electrons aimed at a surface.<sup>10</sup> Such a tip-emitted beam does expand with an angular spread of perhaps  $5^\circ$ , so it is only approximately collimated. While probe diameters of the order of  $40 \mu\text{m}$  across have already been achieved experimentally by this method, the potential exists of exposing regions smaller than about  $40 \text{ nm}$ , close to the size of many nanostructures. We will thus distinguish here between two types of LEED experiment: incident electron beams that are collimated vs convergent.

The cluster representation used in our approach to NANOLEED is naturally suited to handle all the aforementioned cases. The method makes no assumption of any translational symmetry or infinite extent of the sample. We can treat any form of incident wave as a superposition of plane waves with different propagation directions.

We use the case of a SiNW to describe what a LEED pattern due to a nanostructure may look like. For convenience and clarity, we will assume here a single isolated wire, whose supports are outside the incident beam diameter, and a well-collimated incident beam. The left-hand panels of Fig. 1 show LEED patterns expected for periodic one-dimensional (1D), two-dimensional (2D), and three-dimensional (3D) arrays of infinite extent, neglecting electron damping. The patterns displayed in the right-hand panels include all multiple scattering in these Si clusters as well as the effects of Si atomic scattering amplitudes (phase shifts), an inelastic mean free path for electron damping, and thermal vibrations (as described in the next section), so they are quite realistic; the damping, in particular, limits the electron penetration to the first few atomic layers. We select an incident beam direction along the  $0z$  axis towards negative  $z$ .

A single 1D string of atoms has a 1D reciprocal lattice that only restricts momentum transfer parallel to the wire: its diffraction pattern thus consists of infinitely sharp cones with axes along the wire, as shown in the left panels of Figs. 1(a)–1(c) (the spheres represent the Ewald sphere that imposes the incident energy on the elastically scattered electrons): electrons can diffract in any azimuth relative to the wire axis, but only in a restricted set of polar angles relative to that axis, as given by a set of 1D Bragg conditions due to the 1D periodicity. Figures 1(a)–1(c) show the effect of orienting the same wire along three Cartesian axes (the infinite sharpness of the cones assumes strict 1D periodicity; in particular, for the string orientation along  $\pm z$ , this means no damping and negligible forward scattering effects, so each atom receives the same total incident amplitude).

With an incident beam direction along the  $0z$  axis towards negative  $z$ , hemispherical LEED patterns can be observed as shown in the right-hand panels in Fig. 1, displayed in reciprocal space as would be seen in a standard LEED setup with a hemispherical screen (diffraction actually continues

smoothly into the complementary hemisphere below the  $xy$  plane for a finite nanostructure). These patterns also show the effect of limiting the string to a finite length. With finite strings, the infinitely sharp cones broaden into “thicker” cones, i.e., the polar angle relative to the wire axis is no longer strictly limited; the shorter the string, the thicker the cones. The relatively intense straight lines in the right-hand patterns of Fig. 1 correspond directly to the Bragg cones of the left-hand patterns, while the weaker intermediate lines are due to the finite length of the atomic strings: for a chain of  $n$  atoms, there are  $n-2$  weaker lines between intense lines, from basic diffraction principles. The finite-string pattern of Fig. 1(c) shows less Bragg-like structure than the others because the incident beam decays rapidly along the  $z$ -oriented string due to damping and is further perturbed by multiple forward scattering, so this string diffracts in a strongly non-periodic fashion.

The cone broadening is directly analogous to beam broadening due to finite-size domains in conventional LEED, as can also be seen in Fig. 1(d), which assumes a 2D array of  $7 \times 7$  atoms (conventional LEED from a periodic surface, in addition, produces infinitely sharp peaks, at the centers of the broader beams seen here, due to the perfectly periodic substrate). Here, the pattern can be viewed as the intersection of two sets of cones (along the  $x$  and  $y$  axes, respectively), with a “thickness” inversely proportional to the number of atoms in each dimension.

If we now build a simple cube by stacking identical atomic layers, the pattern does not change qualitatively, as seen in Fig. 1(e): the third dimension adds cones oriented along the  $z$  axis (broadened by damping, etc.), which only modulates the intensities further, according to the relatively smooth angle dependence shown in Fig. 1(c).

We next illustrate in Fig. 2 the same type of LEED pattern for more representative Si nanostructures, now assuming the proper diamond lattice, but still ideally terminated at the outer surfaces. We select a  $[1, 1, -2]$  wire axis along  $0x$  and a (111) surface termination toward positive  $z$ . Again, a collimated beam is incident toward negative  $z$ . Figure 2(a) illustrates LEED from a quantum dot with roughly  $2 \times 4 \times 2$  bulk Si unit cells, containing 78 atoms. Figure 2(b) shows the case of a longer but thinner nanostructure with roughly  $13 \times 3 \times 2$  bulk Si unit cells, containing 486 atoms. Figure 2(c) assumes a longer nanowire with roughly  $27 \times 2 \times 2$  bulk Si unit cells, containing 1030 atoms. It is clearly confirmed that the width of the “spots” in the pattern depends inversely on the nanostructure size in the  $x$  and  $y$  directions, allowing the determination of nanostructure size. Compared to Fig. 1, the LEED patterns in Fig. 2 for SiNWs are more complex, due to the diamond structure, vs the simple cubic structure assumed in Fig. 1. Note, in particular, in Fig. 2 the approximately threefold symmetrical pattern expected for the (111) bulk Si termination, seen even with extremely thin nanowires.

Of course, STM and transmission electron microscopy can often evaluate nanostructure size very directly and easily, at least in two dimensions and sometimes also in three dimensions. However, the different techniques may not be able to investigate the same given nanostructure sample in exactly the same environment in the same vacuum chamber, so an independent analysis of nanostructure size by LEED remains useful.

## LEED patterns for simple nanostructures

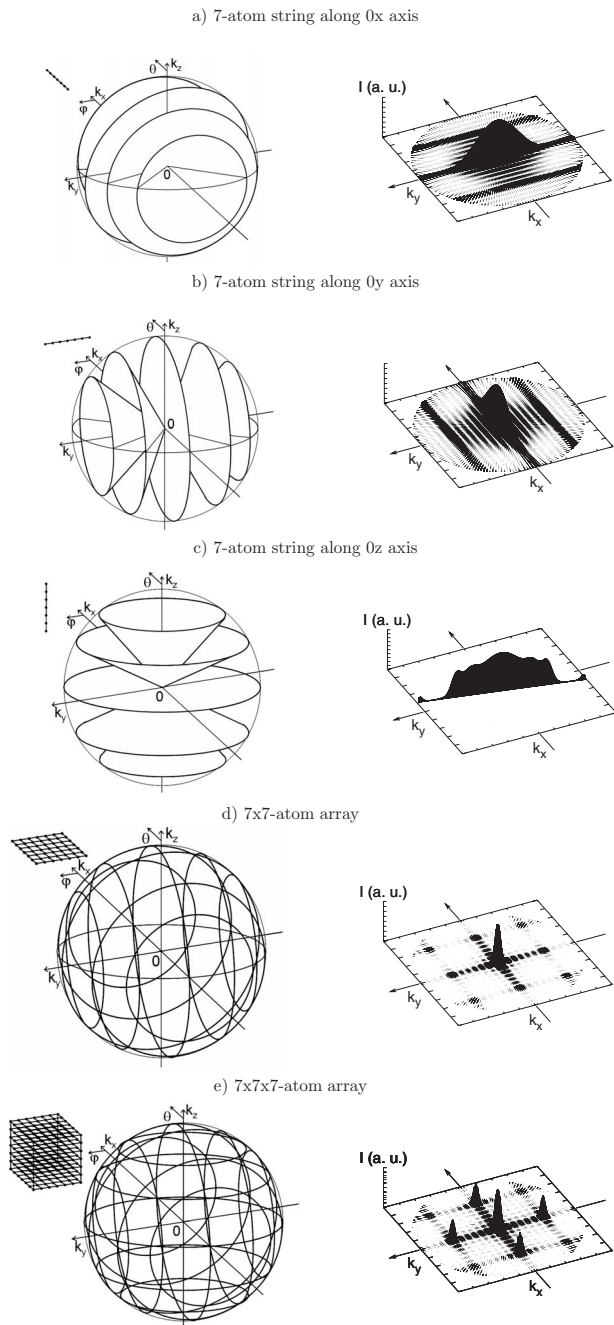


FIG. 1. Examples of LEED patterns in reciprocal space for simple nanostructures made of Si atoms (sketched at far left), of both infinite size (left panels) and finite size (right panels): a string of Si atoms along (a)  $\pm x$ , (b)  $\pm y$ , and (c)  $\pm z$ ; (d) a planar square grid; and (e) a simple cubic grid. The cones in the left-hand panels represent 1D Bragg conditions; they intersect Ewald spheres imposing energy conservation. The right-hand panels show two-dimensional patterns as would be seen in a standard LEED setup, as intensity vs parallel momentum; multiple-scattering intensities are calculated using our method for NANOLEED, using a Si-Si closest distance of 0.3 nm, an electron energy of 100 eV, and a damping of 4 eV. In the right-hand panel of (c) only one profile is shown; the complete pattern is obtained by rotating this profile around the  $z$  axis.

One important class of structural change in nanostructures consists in a uniform elongation or compression compared to the bulk material. This can easily be identified through a change in the cone apertures discussed above: the cone aperture angles are given by the Bragg conditions in each direction and thus also depend on the lattice constant in each direction. These can be easily measured in an angular scan. More subtle effects, such as local elongations and compressions, may also be detectable in such angle-scanned patterns in the form of skewing of peaks, etc.

In practice, it may be useful to first explore such structural effects qualitatively, namely, without making full multiple-scattering calculations. Indeed, many of these effects can already be seen in the single-scattering (kinematic) limit, even if only roughly. Our NANOLEED code allows this option, thereby saving much computer time. After such kinematic modeling, multiple-scattering calculations may be employed to further explore details with higher accuracy, guided by the kinematic results. The next section provides the theory for such multiple-scattering calculations.

## III. THEORY

Here, we first develop the general theory of LEED for an arbitrary convergent incident beam.

Let us choose a geometrical reference point  $O$  and, for convenience, let us assume that it is contained inside the nanosample. The analyzer is then at  $\vec{R}$  with respect to  $O$ . A convergent beam of electrons can be seen as a conical continuum superposition of plane waves  $\phi(\vec{k}_i; \vec{r}) = \frac{1}{(2\pi)^{3/2}} \exp(i\vec{k}_i \cdot \vec{r})$ . If each of these beams has its own amplitude  $A(\vec{k}_i)$ , and the cone of beams is centered on the direction  $\vec{k}_{i0}$  and has an angular opening  $\Omega_{inc}$ , the total incident electron wave function can be written as

$$\begin{aligned} \Psi_{inc}(\vec{k}_{i0}, \Omega_{inc}; \vec{r}) &= \int_{\Omega_{inc}} A(\vec{k}_i) \phi(\vec{k}_i; \vec{r}) d\vec{k}_i \\ &= \frac{1}{(2\pi)^{3/2}} \int_{\Omega_{inc}} A(\vec{k}_i) \exp(i\vec{k}_i \cdot \vec{r}) d\vec{k}_i. \end{aligned}$$

The intensity of the scattered beam is proportional to the scattering differential cross section  $(d\sigma/d\Omega)(\Omega_a)$  calculated for the direction  $\Omega_a \equiv (\theta_a, \varphi_a)$  of the analyzer. The differential cross section is proportional to the square modulus of the angular part of the scattered wave function, which can be obtained using the Lippmann-Schwinger equation

$$\Psi_{sc} = \Psi_{inc} + G_0 T \Psi_{inc},$$

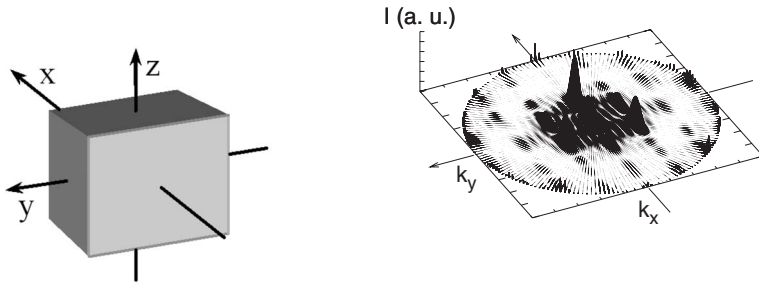
where  $G_0$  is the electron's vacuum propagator and  $T$  is the total transition (scattering) operator of the nanostructure studied. In the case of a LEED experiment, however, only the reflected electrons are recorded, so the above equation becomes

$$\Psi_{sc} = G_0 T \Psi_{inc}.$$

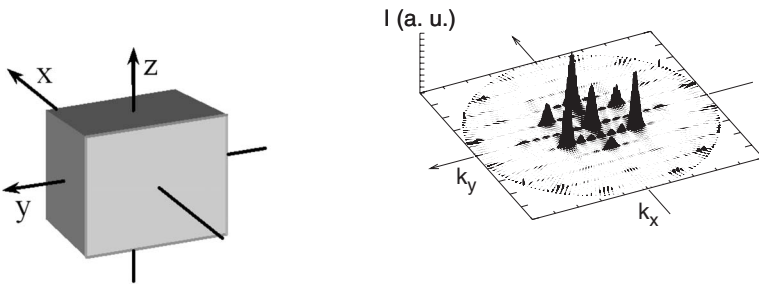
After some manipulations, one finds that the scattered waves can be written in terms of spherical harmonics as

LEED patterns for different Si nanostructures

a) Si quantum dot : 0.9nm x 1.6nm x 0.7nm



b) Short & thick Si nanowire : 4.9nm x 1.2nm x 0.7nm



c) Long & thin Si nanowire : 10.2nm x 0.8nm x 0.7nm

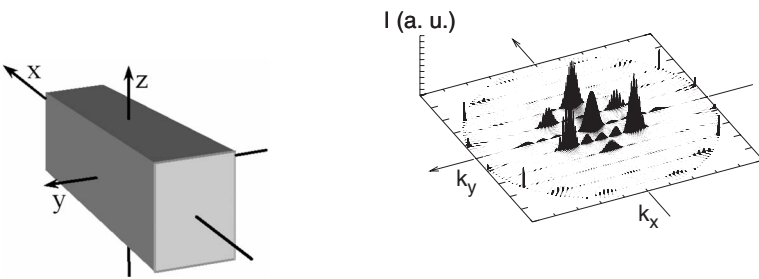


FIG. 2. The influence of nanostructure size (left panels) on the LEED pattern (right panels) for three sample SiNWs. Assumed is an ideally terminated bulk Si structure with  $[1, 1, -2]$  growth direction along  $\pm x$  and a (111) surface exposed toward positive  $z$ . From (a) to (c), the length (along  $x$ ) increases and the width (along  $y$ ) decreases as indicated.

$$\Psi_{sc}(\vec{R}) = -i \sqrt{\frac{\pi}{2}} \frac{1}{k_0} \sum_{i,L,L'} \int_0^{4\pi} i^{l'} h_{l'}^{(1)} \times (k_0 R) Y_{L'}(\hat{R}) Y_{L'}^*(\hat{\kappa}) Y_L(\hat{\kappa}) \exp(-i \vec{\kappa} \vec{R}_i) d\hat{\kappa} X_L^i(k_0, \vec{R}_i, \Omega_{inc}),$$

where  $(1/2)k_0^2$  is the kinetic energy of the elastically scattered electrons,  $\vec{R}_i$  is the geometrical position of atom  $i$  with respect to the chosen geometrical reference point  $O$ ,  $h_l^{(1)}(z)$  is a spherical Hankel function of the first kind,  $Y_L(\hat{x})$  is a spherical harmonic,  $\hat{x}$  is the unit vector in the direction of  $\vec{x}$ , the sum over  $i$  runs from 1 to the total

number of atoms in the nanostructure, and  $X_L^i(k_0, \vec{R}_i, \Omega_{inc}) = \sum_{L'} \int_{\Omega_{inc}} A(\vec{k}_i) \exp(i \vec{k}_i \vec{R}_i) Y_{L'}^*(\hat{k}_i) d\hat{k}_i T_{i,L,L'}(k_0)$  is the individual contribution of each of the nanosystem's atoms to the total scattering wave function. This vector is the solution of the multiple-scattering equations of the electron inside the nanosystem. The actual technique used to solve the equations was described in our previous paper.<sup>2</sup> For the SiNW system, there is one complication that arises in the calculation: the multiple scattering between Si and H atoms can be strong and, as a result, the method does not always converge. However, if the small cluster formed by a Si atom and its closest H neighbors (no more than 3 in our case) are treated as a single “pseudoatom” cluster characterized by a nondiagonal scattering

matrix,<sup>11</sup> the calculations converge well. In this case, the multiple-scattering equation inside the pseudoatom has to be solved exactly by matrix inversion.

As the distance from the sample to the analyzer is very large compared to any interatomic distance involved in the formulas above, the spherical Hankel functions of the first kind present in the calculation can be replaced by their asymptotical forms:

$$i^{l+1}h_l^{(1)}(x) \xrightarrow{x \rightarrow \infty} \frac{\exp(ix)}{x}.$$

With  $\vec{\kappa}_{sc} = k_0 \hat{R}_{sc}$ , we thus obtain

$$\begin{aligned} \Psi_{sc}(\vec{R}) = & -\sqrt{\frac{\pi}{2}} \frac{1}{k_0^2 R} \sum_{i,L} \exp(ik_0 R) \exp(-i\vec{\kappa}_{sc} \vec{R}_i) \\ & \times Y'_L(\hat{\kappa}_{sc}) X'_L(k_0, \vec{R}_i, \Omega_{inc}). \end{aligned}$$

Using the notation

$$f(\theta_a, \varphi_a) \equiv -\sqrt{\frac{\pi}{2}} \frac{1}{k_0^2} \sum_{i,L} \exp(-i\vec{\kappa}_{sc} \vec{R}_i) Y'_L(\hat{\kappa}_{sc}) X'_L(k_0, \vec{R}_i, \Omega_{inc}),$$

which gives the scattering amplitude of the nanosystem, one finds for the scattered wave function the expression

$$\Psi_{sc}(\vec{R}) = \frac{\exp(ik_0 R)}{R} f(\theta_a, \varphi_a),$$

similar to the familiar atomic scattering result.<sup>12</sup>

In terms of incident and scattered fluxes, the differential cross section can be written<sup>12</sup> as

$$\frac{d\sigma}{d\Omega}(\Omega_a) = \frac{d\Phi_{sc}}{\Phi_{inc} d\Omega}(\Omega_a),$$

with

$$\Phi_{inc} = \int_{\Omega_{inc}} \vec{j}_{inc}(\hat{k}_i) \cdot \hat{k}_i d\hat{k}_i = \frac{k_0}{(2\pi)^3} \int_{\Omega_{inc}} |A(\hat{k}_i)| d\hat{k}_i,$$

$$\Phi_{sc} = \vec{j}_{sc} \cdot \hat{R} R^2 d\Omega = k_0 |f(\Omega_a)|^2 d\Omega,$$

where

$$\vec{j}(\vec{r}) = \text{Re} \left\{ \frac{1}{i} \Psi^*(\vec{r}) \vec{\nabla} \Psi(\vec{r}) \right\}$$

and  $R^2 d\Omega$  is the acceptance area of the analyzer's aperture.

The final expression of the differential cross section is then

$$\frac{d\sigma}{d\Omega}(\Omega_a) = (2\pi)^3 \frac{|f(\Omega_a)|^2}{\int_{\Omega_{inc}} |A(\hat{k}_i)|^2 d\hat{k}_i}.$$

In the case of a normal LEED experiment (parallel incident beam), this formula becomes

Axial elongation of a SiNW  
Beam=(0,0)

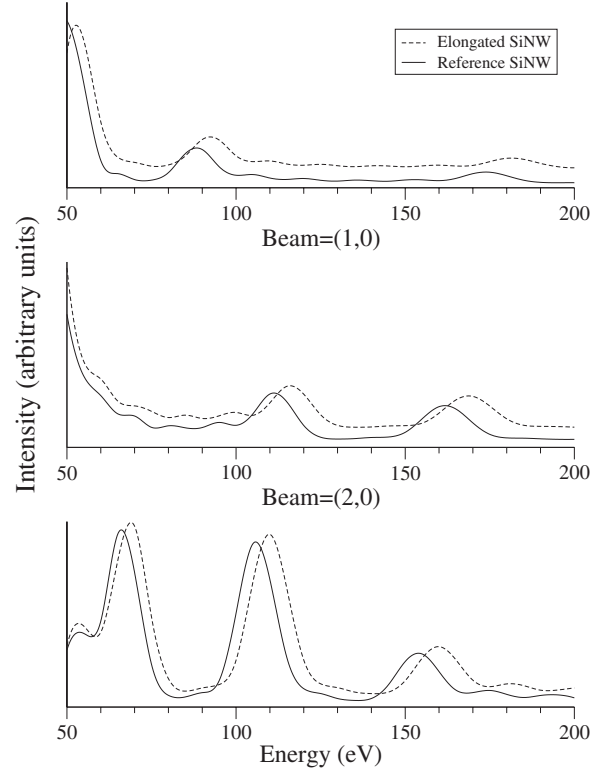


FIG. 3. Effect on LEED  $I$ - $V$  curves of a uniform 4% elongation (dashed lines) of a bulk-terminated SiNW relative to a bulklike geometry (full lines). The initial nanowire dimensions are  $10.2 \times 0.8 \times 0.7 \text{ nm}^3$ , as in Fig. 2(c). The wire thickness decreases with elongation to conserve volume. The beam labeling follows standard LEED practice for extended surfaces, such that the (0,0) beam represents specular reflection from the (111) upper surface of the wire (this beam or spot appears at the center of the right-hand patterns in Figs. 1 and 2).

$$\frac{d\sigma}{d\Omega}(\Omega_a) = (2\pi)^3 |f(\Omega_a)|^2,$$

with the changed definition

$$\begin{aligned} X'_L(k_0, \vec{R}_i, \Omega_{inc}) & \rightarrow X'_L(k_0, \vec{R}_i, \vec{k}_i) \\ & = \sum_{L'} \exp(i\vec{k}_i \vec{R}_i) Y_{L'}^*(\hat{k}_i) T_{i,L,L'}(k_0). \end{aligned}$$

#### IV. NANOLEED CALCULATIONS: APPLICATION TO SILICON NANOWIRES

Besides nanostructure size, dealt with in Sec. II, we wish to also be able to study other structural aspects, such as deviations of bond lengths from the bulk structure, reconstructions, and adsorption geometry. Similar to conventional LEED applied to extended surfaces, NANOLEED should also have that potential. We will show this to be the case in this section by distorting a SiNW from its ideal bulklike structure

LEED patterns for different (111) surface terminations  
of a [112] SiNW

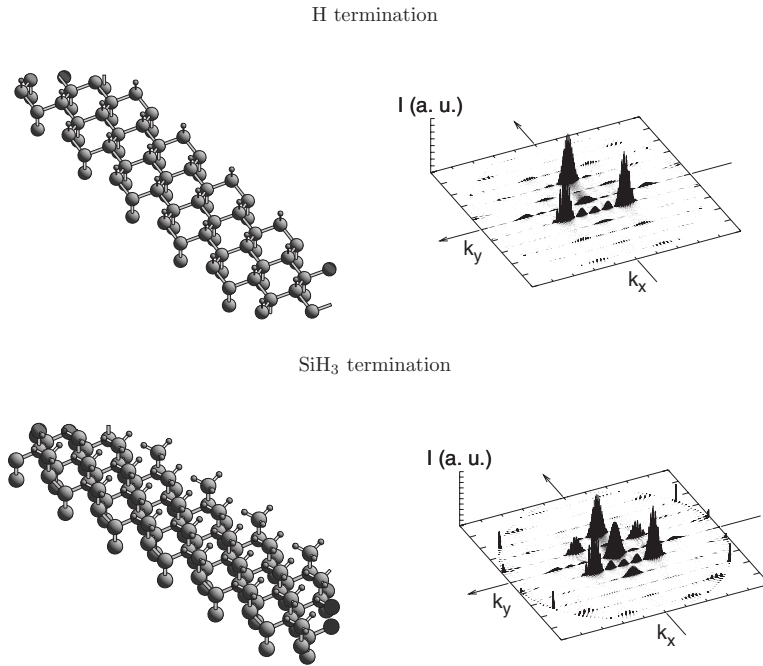


FIG. 4. LEED patterns for H termination (top panels) and  $\text{SiH}_3$  termination (bottom panels) of SiNWs with  $[1, 1, -2]$  growth direction. This termination is applied only to the upper (111) surface, as illustrated on the left.

and observing the effect on LEED intensities, as calculated by our method.

In order to investigate the above-mentioned LEED patterns and to test our predictions on the method's sensitivity to nanoscale structural changes, we have chosen as nanosystem an isolated single SiNW, pure or hydrogen terminated. This type of nanowire can be experimentally grown<sup>3</sup> on a HOPG substrate, and total energy calculations have shown<sup>5</sup> that the stable cross section of a H-terminated SiNW is likely rectangular. Guided by experiment, in particular, STM images,<sup>3</sup> we select a SiNW with a  $[1, 1, -2]$  direction of growth: STM shows its (111) facet exposed, and thus, its side facets would have  $\{1-10\}$  orientation. We will assume unreconstructed Si facets, as observed by STM, due to the H saturation: clearly, NANOLEED could also be used very well to study details of such facet reconstruction, if present. In this application, we ignore the supporting substrate (HOPG), but it could be included if desired.

In our modeling, we use silicon phase shifts calculated for bulk silicon and hydrogen phase shifts calculated for H adsorbed on Si. Thermal vibrations for room temperature are modeled through the customary Debye-Waller factor, using a bulk Si Debye temperature. A muffin-tin zero of  $-10$  eV is used, and an electron "damping" is included as usual through an imaginary part of the potential, with the value of 5 eV. The muffin-tin zero and damping only act inside the outer envelope of the sample.

As mentioned earlier, one could focus an electron beam onto a single SiNW. If the resulting beam has a sizable angular spread, as in convergent-beam LEED,<sup>6</sup> then the diffraction pattern will be correspondingly broadened: this would still be valuable if this spread is taken into account in the calculation through convolution (as is already commonly

done in photoelectron diffraction,<sup>13</sup> for example). In that situation, the same structural information is present in the pattern, although convoluted, both in the experiment and in the theory: fitting theory to experiment can still determine unknown structural parameters.

In the following, for simplicity, we will neglect the angular spread of the incident beam and concentrate on the features specific to a SiNW's diffraction pattern.

The primary structure-sensitive feature of conventional LEED is the " $I$ - $V$  curve," which presents a beam intensity as a function of incident beam energy, i.e., accelerating voltage  $V$ . Note that the exit angle of a beam varies with energy, so the beam direction must also be followed when measuring an  $I$ - $V$  curve. We can use the familiar  $(h, k)$  notation for beams in the case of a bulk-derived nanostructure [these beams form the 2D array of relatively intense spots in the patterns of Figs. 1(d), 1(e), and 2].

NANOLEED patterns are inherently diffuse (they have non-zero intensity essentially everywhere), so they offer more opportunities to use angle-scanned measurements and calculations, relative to conventional LEED from ordered 2D surfaces. Diffracted intensities can be measured under a variety of rotations, depending on the degrees of freedom of the instrumentation: for example, the nanostructure can be rotated around the incident beam direction or around any of its own axes, or the detector can be rotated by itself along various arcs. Each such rotation will be more or less sensitive to some structural feature of the nanostructure, depending on the particular type of nanostructure. Furthermore, the conventional hemispherical LEED display provides a two-dimensional data set that includes several of those rotations: similar to photoelectron diffraction, it is also possible to use the entire 2D pattern as a single data set without slicing it up into arcs.

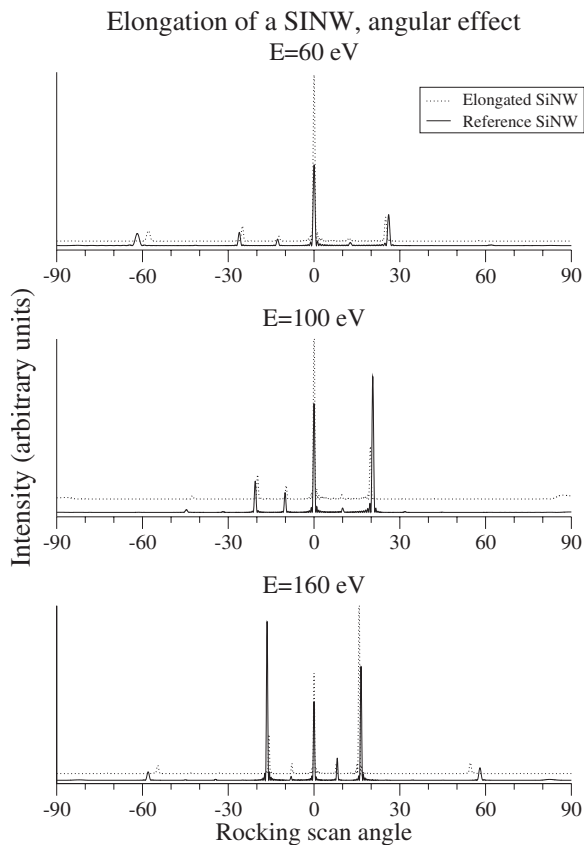


FIG. 5. Effect of a uniform 4% elongation of a  $\text{SiH}_3$ -terminated SiNW on LEED “rocking” scans at three different incident electron energies. The elongation is performed as in Fig. 3. The scans rotate the detector in the  $xz$  plane of Fig. 4, with  $0^\circ$  along the  $z$  axis marking specular reflection from the top of our SiNW.

In Sec. II, we addressed the effect of elongation or compression of a nanostructure compared to the bulk. Besides the effect on angular scans, it can also be seen in  $I$ - $V$  curves, as shown in Fig. 3 for three relatively intense beams. As with conventional LEED,  $I$ - $V$  curves are most sensitive to spacings perpendicular to the momentum transfer, in this case along the  $z$  axis. Thus, with an elongation along the  $x$  axis, if we assume a corresponding compression along the  $y$  and  $z$  axes (to maintain a constant 3D unit-cell volume), spacings will be reduced along the  $z$  axis, yielding a shift toward larger energies of features in  $I$ - $V$  curves, as is visible in Fig. 3. This behavior is seen to be the same as in conventional LEED from extended surfaces.

Our next calculations illustrate sensitivity to adsorption and surface termination. It is believed that the SiNWs which we model here are, in reality, hydrogen terminated, and we can show that NANOLEED can clearly distinguish different modes of H termination. Total energy calculations<sup>5</sup> show that two terminations are possible for the (111) facet of the  $[11\bar{2}]$  SiNW, with little difference in total energy: a “H termination,” in which a single H saturates a surface Si atom, and a “ $\text{SiH}_3$  termination,” in which each such H atom is replaced by a  $\text{SiH}_3$  group (representing a different cut of the substrate), as illustrated on the left in Fig. 4. The right-hand panels of Fig. 4 show that the LEED patterns corresponding

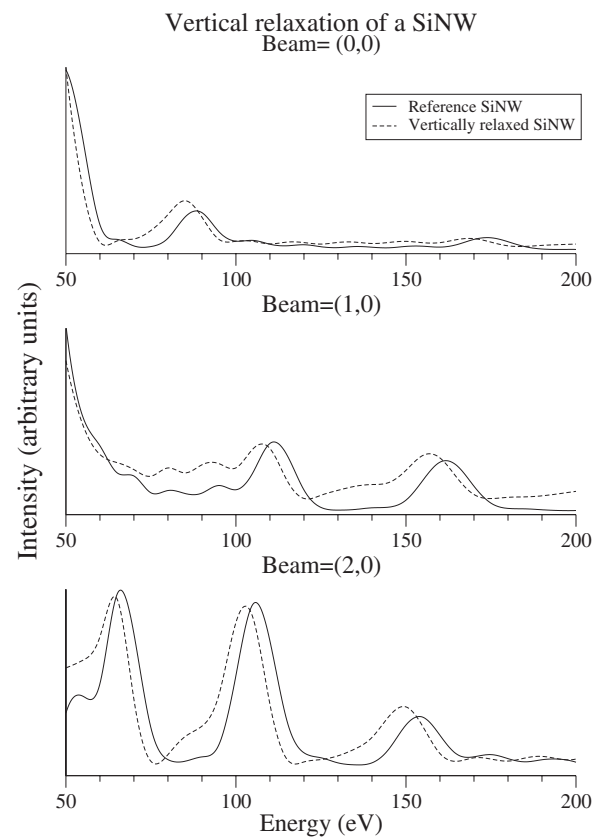


FIG. 6. Effect on  $I$ - $V$  curves of an outward displacement by 0.01 nm along the  $z$  axis of the  $\text{SiH}_3$  layer in the  $\text{SiH}_3$ -terminated SiNW of Fig. 4.

to the single H termination and to the  $\text{SiH}_3$  termination are distinctly different. It should be noted, as with the corresponding extended-surface structure, that the LEED intensities are only weakly sensitive to the H atoms themselves: here, it is mainly the additional Si atom that distinguishes the two cases.

Since the  $\text{SiH}_3$  termination is energetically slightly more favorable than the H termination, for the rest of this paper, we will only consider  $\text{SiH}_3$ -terminated SiNWs in our test calculations.

We next explore the sensitivity of our method to various nanoscale changes in a SiNW’s geometry. We will focus on sensitivity to deformations caused by relaxation and by interaction with external forces. The system of study will always be the long, thin,  $\text{SiH}_3$ -terminated nanowire previously described [see Fig. 2(c)].

As discussed earlier, a change in the length of the 1D “unit cell” of the nanowire will alter the positions of the Bragg maxima, which should leave its mark both on the  $I$ - $V$  curves and on angular scans. To test this, we imagine a force that elongates the wire along its axis, such that the length of its unit cell increases by 4% (the unit cell is 0.67 nm long, increased by the imaginary force by about 0.028 nm). We suppose that the wire further changes its shape in order to preserve its total volume, leading to shrinking of size in the two transverse directions by about 0.015 nm. Indeed, as Figs. 3 and 5 show, this type of elastic deformation leads to significant responses in both  $I$ - $V$  curves (Fig. 3) and angular

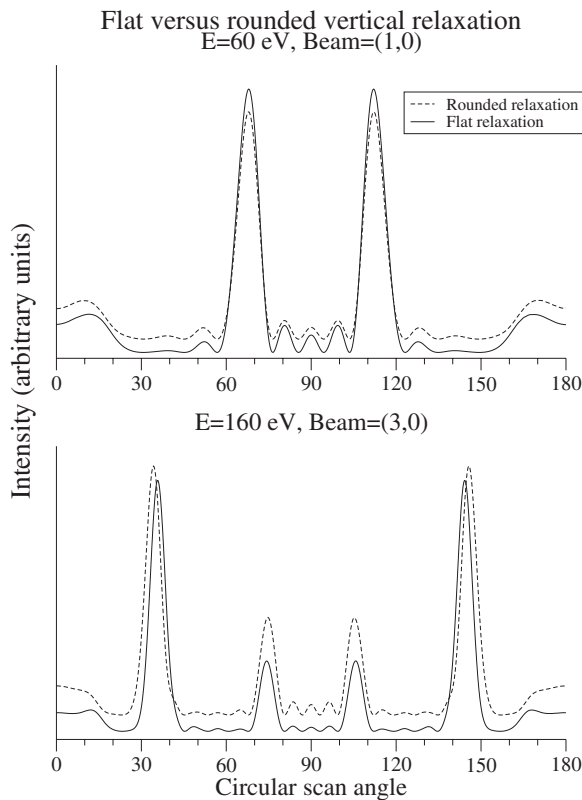


FIG. 7. Effect on LEED intensities of “rounding” the relaxation (used in Fig. 6) of the topmost SiH<sub>3</sub> layer in our SiNW, as described in the text. Shown are “circular” scans around the long axis of the nanowire, with 90° along the *z* axis marking specular reflection from the top facet of our SiNW.

“rocking scans” (Fig. 5). The angular scans show sharp peaks due to the length of the SiNW; these peaks occur at Bragg angles, which, of course, depend on energy.

The question of how a nanostructure deviates from the bulk structure is certainly of great importance. In order to prove that NANOLEED can be a useful tool to study these phenomena, we imagine a relaxation such that the SiH<sub>3</sub> terminal layer moves outward, increasing the distance to the

next Si layer by 0.01 nm. Figure 6 proves that the NANOLEED *I-V* curves show significant response to relaxation, similar to conventional LEED.

In the preceding relaxation, we assumed that the entire SiH<sub>3</sub> layer moves rigidly, neglecting that the displacement could be different near the edges of the nanowire, where its (111) facets terminate: in reality, the nanowire cross section could, for example, become rounded. To explore this possibility, we assume that the SiH<sub>3</sub> groups near the edges move outward by 0.008 nm and those toward the middle of the facets move outward by 0.012 nm, with intermediate relaxations in between. We have performed NANOLEED calculations in order to determine whether our method can distinguish the uniform from the rounded relaxation model, despite the small structural differences involved (a maximum of only 0.002 nm in relative displacements). We have found that the *I-V* curves show very little sensitivity to this “rounding.” However, “circular” detector scans around the nanowire axis show satisfactory sensitivity, as shown in Fig. 7: note, in particular, the peak shifts at 160 eV. Thus our method has the potential to investigate even such subtle relaxation mechanisms in the case of nanowires.

Up to now, we have proven the sensitivity of our method to extensive changes in the studied system’s geometry. We have shown how the *I-V*, rocking and circular, scans respond to nanostructural changes involving a large number of atoms. However, sensitivity to local, nanosized defects, involving a small number of atoms located in a small area, would also be very welcome. To explore this potential, we imagine a local defect in our SiNW and try to detect it by NANOLEED. Our defect is a small dip or depression on one side of the nanowire: we inwardly compress the outermost atoms of the lateral (1, -1, 0) facet by 0.04 nm over a length of only 0.67 nm (one 1D unit cell of the SiNW). Thus we move eight Si atoms and ten H atoms (out of 1030 atoms in the 10.2-nm-long nanowire) by 0.04 nm perpendicularly to the incident beam, a very challenging situation for LEED. We ran NANOLEED simulations to test whether this “defect” geometry produces detectable responses in any type of curve. The *I-V*, rocking and circular, curves showed no significant sensitivity to this particular kind of structural change. How-

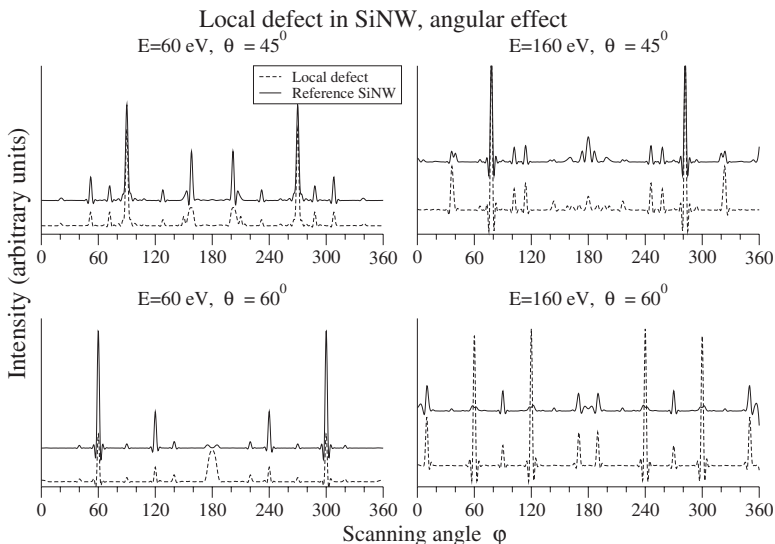


FIG. 8. Effect on LEED intensities of a small defect in our SiNW, as described in the text. Shown are azimuthal scans with fixed scattering angle calculated for 60 eV, considering fixed polar angles of 45° and 60° with respect to the incident electron beam.

ever, azimuthal scans with fixed scattering angle ( $360^\circ$  angular scans with constant polar angle around the incident beam direction), shown in Fig. 8, offer a good response in the presence of our nanoscale defect. These encouraging results open up the possibility of using NANOLEED to investigate nanoscale defects.

Given the encouraging results of this work, we propose that NANOLEED be applied to actual structure determination, as soon as suitable experimental data are available. As is well known, an important tool of structural determination with LEED is an automated optimization method capable of maximizing the good fit to experiment in the presence of many unknown structural parameters. We are currently developing such a method for NANOLEED.<sup>11</sup>

## V. CONCLUSIONS

This paper has described the potential of our method, "NANOLEED," to analyze the detailed atomic-scale structure of individual nanostructures. With the example of silicon nanowires, we have shown that it should be possible to determine size, shape, lattice constant, surface terminations, re-

laxations, adsorption geometry, etc., the latter much as with conventional LEED applied to extended surfaces.

Our multiple-scattering theory includes the possibility to handle noncollimated incident electrons beams, as with the proposed convergent-beam LEED and STM-based LEED, both of which are suitable for studying nanoscale objects. We suggest that instrumentation be developed to perform such LEED intensity measurements.

It is also suggested that kinematic (single-scattering) LEED can be used for the initial analysis of a nanostructure. This, in particular, allows a low-cost exploration to determine which form of experimental data ( $I$ - $V$  curves or any of various angle scans) can provide the maximum sensitivity to desired structural information for a specific kind of nanostructure.

## ACKNOWLEDGMENTS

This work was supported by RGC Grant No. CityU1/02C, and in part by the Office of Science, Materials Sciences Division, of the U.S. Department of Energy under Contract No. DE-AC03-76SF00098 while M.A.V.H. was at Lawrence Berkeley National Laboratory.

<sup>1</sup>G. M. Gavaza, Z. X. Yu, L. Tsang, C. H. Chan, S. Y. Tong, and M. A. Van Hove, *Phys. Rev. Lett.* **97**, 055505 (2006).

<sup>2</sup>G. M. Gavaza, Z. X. Yu, L. Tsang, C. H. Chan, S. Y. Tong, and M. A. Van Hove, *Phys. Rev. B* **75**, 014114 (2007).

<sup>3</sup>D. D. D. Ma, C. S. Lee, F. C. K. Au, S. Y. Tong, and S. T. Lee, *Science* **299**, 874 (2003).

<sup>4</sup>J. Niu, J. Sha, and D. Yang, *Physica E (Amsterdam)* **23**, 131 (2004).

<sup>5</sup>R. Q. Zhang, Y. Lifshitz, D. D. D. Ma, Y. L. Zhao, Th. Frauenheim, S. T. Lee, and S. Y. Tong, *J. Chem. Phys.* **123**, 144703 (2005).

<sup>6</sup>J. C. Spence, H. C. Poon, and D. K. Saldin, *Microsc. Microanal.* **10**, 128 (2004).

<sup>7</sup>M. A. Van Hove and S. Y. Tong, *Surface Crystallography by LEED* (Springer-Verlag, Berlin, 1979).

<sup>8</sup>M. A. Van Hove, W. H. Weinberg, and C. M. Chan, *Low-Energy Electron Diffraction* (Springer-Verlag, Berlin, 1986).

<sup>9</sup>See, for example, D. K. Saldin, J. B. Pendry, M. A. Van Hove, and G. A. Somorjai, *Phys. Rev. B* **31**, 1216 (1985); G. S. Blackman, M.-L. Xu, D. F. Ogletree, M. A. Van Hove, and G. A. Somorjai, *Phys. Rev. Lett.* **61**, 2352 (1988).

<sup>10</sup>S. Mizuno, F. Rahman, and M. Iwanaga, *Jpn. J. Appl. Phys., Part 2* **45**, L178 (2006).

<sup>11</sup>M. A. Van Hove, G. M. Gavaza, and Z. X. Yu (unpublished).

<sup>12</sup>C. J. Joachain, *Quantum Collision Theory* (North-Holland, Amsterdam, 1975).

<sup>13</sup>C. S. Fadley, Y. Chen, R. E. Couch, H. Daimon, R. Denecke, J. D. Denlinger, H. Galloway, Z. Hussain, A. P. Kaduwela, Y. J. Kim, P. M. Len, J. Liesegang, J. Menchero, J. Morais, J. Palomares, S. D. Ruebush, E. Rotenberg, M. B. Salmeron, R. Scalettar, W. Schattke, R. Singh, S. Thevuthasan, E. D. Tober, M. A. Van Hove, Z. Wang, and R. X. Ynzunza, *Prog. Surf. Sci.* **54**, 341 (1997).